Bhaskar Chandra Sarkar, Sanatan Das, Rabindra Nath Jana / International Journal of Engineering Research and Applications (IJERA) ISSN: 2248-9622 www.ijera.com
Vol. 2, Issue4, July-August 2012, pp.2346-2359

Effects of Radiation on MHD Free Convective Couette Flow in a Rotating System

Bhaskar Chandra Sarkar[1], Sanatan Das[2] and Rabindra Nath Jana[3]
[1,3](Department of Applied Mathematics,Vidyasagar University, Midnapore 721 102, India)
[2](Department of Mathematics, University of Gour Banga, Malda 732 103, India)

ABSTRACT

The effects of radiation on MHD free convection of a viscous incompressible fluid confined between two vertical walls in a rotating system have been studied. We have considered the flow due to the impulsive motion of one of the walls and the flow due to accelerated motion of one of the walls. The governing equations have been solved analytically using the Laplace transform technique. The variations of fluid velocity components and fluid temperature are presented graphically. It is found that the primary velocity decreases whereas the secondary velocity increases for both the impulsive as well as the accelerated motion of one of the walls with an increase in either magnetic parameter or radiation parameter. There is an enhancement in fluid temperature as time progresses. The absolute value of the shear stresses at the moving wall due to the primary and the secondary flows for both the impulsive and the accelerated motion of one of the walls increase with an increase in either rotation parameter or radiation parameter. The rate of heat transfer at the walls increases as time progresses.

Keywords: **MHD Couette flow, free convection, radiation, rotation, Prandtl number, Grashof number, impulsive motion and accelerated motion.**

I. INTRODUCTION

Couette flow is one of the basic flow in fluid dynamics that refers to the laminar flow of a viscous fluid in the space between two parallel plates, one of which is moving relative to the other. The flow is driven by virtue of viscous drag force acting on the fluid. The radiative convective flows are frequently encountered in many scientific and environmental processes such as astrophysical flows, water evaporation from open reservoirs, heating and cooling of chambers and solar power technology. Heat transfer by simultaneous radiation and convection has applications in numerous technological problems including combustion, furnace design, the design of high temperature gas cooled nuclear reactors, nuclear reactor safety, fluidized bed heat exchanger, fire spreads, solar fans, solar collectors, natural convection in cavities, turbid water bodies, photo chemical reactors and many others. The hydrodynamic rotating flow of an electrically conducting viscous incompressible fluid has gained considerable attention because of its numerous applications in physics and engineering. In geophysics, it is applied to measure and study the positions and velocities with respect to a fixed frame of reference on the surface of earth, which rotates with respect to an inertial frame in the presence of its magnetic field. The free convection in channels formed by vertical plates has received attention among the researchers in last few decades due to it's widespread importance in engineering applications like cooling of electronic equipments, design of passive solar systems for energy conversion, design of heat exchangers, human comfort in buildings, thermal regulation processes and many more. Many researchers have worked in this field such as Singh [1], Singh et. al. [2], Jha et.al. [3], Joshi [4], Miyatake et. al. [5], Tanaka et. al. [6]. The transient free convection flow between two vertical parallel plates has been investigated by Singh et al. [7]. Jha [8] has studied the natural Convection in unsteady MHD Couette flow. The radiative heat transfer to magnetohydrodynamic Couette flow with variable wall temperature has been investigated by Ogulu and Motsa [9]. The radiation effects on MHD Couette flow with heat transfer between two parallel plates have been examined by Mebine [10]. Jha and Ajibade [11] have studied the unsteady free convective Couette flow of heat generating/absorbing fluid. The effects of thermal radiation and free convection on the unsteady Couette flow between two vertical parallel plates with constant heat flux at one boundary have been studied by Narahari [12]. Kumar and Varma [13] have studied the radiation effects on MHD flow past an impulsively started exponentially accelerated vertical plate with variable temperature in the presence of heat generation. Rajput and Pradeep [14] have presented the effect of a uniform transverse magnetic field on the unsteady transient free convection flow of a viscous incompressible electrically conducting fluid between two infinite vertical parallel plates with constant temperature and Variable mass diffusion. Rajput and Kumar [15] have discussed combined effects of rotation and radiation on MHD flow past an impulsively started

vertical plate with variable temperature. Das et. al. [16] have investigated the radiation effects on free convection MHD Couette flow started exponentially with variable wall temperature in presence of heat generation. Effect of radiation on transient natural convection flow between two vertical walls has been discussed by Mandal et al.[17].

In the present paper, we have studied the effects of radiation on free convective MHD Couette flow of a viscous incompressible electrically conducting fluid in a rotating system in the presence of an applied transverse magnetic field. It is observed that the primary velocity u_1 decreases whereas the secondary velocity v_1 increases for both the impulsive as well as the accelerated motion of one of the walls with an increase in either magnetic parameter M^2 or radiation parameter R. The fluid temperature decreases with an increase in either radiation parameter R or Prandtl number Pr whereas it increases with an increase in time τ. The absolute value of the shear stress τ_{x_0} due to the primary flow and the shear stress τ_{y_0} due to the secondary flow at the wall $(\eta = 0)$ for both the impulsive and the accelerated motion of one of the walls increase with an increase in either radiation parameter R or rotation parameter K^2. Further, the rate of heat transfer $-\theta'(0)$ at the wall $(\eta = 0)$ increases whereas the rate of heat transfer $-\theta'(1)$ at the wall $(\eta = 1)$ decreases with an increase in radiation parameter R.

II. FORMULATION OF THE PROBLEM AND ITS SOLUTIONS

Consider the unsteady free convection MHD Couette flow of a viscous incompressible electrically conducting fluid between two infinite vertical parallel walls separated by a distance h. Choose a cartesian co-ordinates system with the x-axis along one of the walls in the vertically upward direction and the z-axis normal to the walls and the y-axis is perpendicular to xz-plane [See Fig.1]. The walls and the fluid rotate in unison with uniform angular velocity Ω about z axis. Initially, at time $t \le 0$, both the walls and the fluid are assumed to be at the same temperature T_h and stationary. At time $t > 0$, the wall at $(z = 0)$ starts moving in its own plane with a velocity $U(t)$ and is heated with the temperature $T_h + (T_0 - T_h)\frac{t}{t_0}$, T_0 being the temperature of the wall at $(z = 0)$ and t_0 being constant. The wall at $(z = h)$ is stationary and maintained at a constant temperature T_h. A uniform magnetic field of strength B_0 is imposed perpendicular to the walls. It is also assumed that the radiative heat flux in the x-direction is negligible as compared to that in the z- direction. As the walls are infinitely long, the velocity field and the fluid temperature are functions of z and t only.

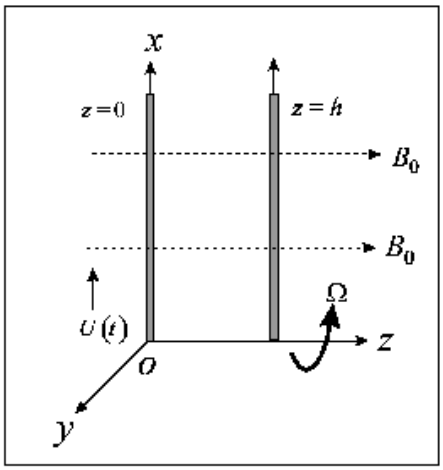

Fig.1: Geometry of the problem.

Under the usual Boussinesq's approximation, the fluid flow be governed by the following system of equations:

$$\frac{\partial u}{\partial t} - 2\Omega v = \nu \frac{\partial^2 u}{\partial z^2} + g\beta^*(T - T_h) - \frac{\sigma B_0^2}{\rho} u, \quad (1)$$

$$\frac{\partial v}{\partial t} + 2\Omega u = \nu \frac{\partial^2 v}{\partial z^2} - \frac{\sigma B_0^2}{\rho} v, \quad (2)$$

$$\rho c_p \frac{\partial T}{\partial t} = k \frac{\partial^2 T}{\partial z^2} - \frac{\partial q_r}{\partial z}, \quad (3)$$

where u is the velocity in the x-direction, v is the velocity in the y-direction, g the acceleration due to gravity, T the fluid temperature, T_h the initial fluid temperature, β^* the coefficient of thermal expansion, ν the kinematic coefficient of viscosity, ρ the fluid density, σ the electric conductivity, k the thermal conductivity, c_p the specific heat at constant pressure and q_r the radiative heat flux.

The initial and the boundary conditions for velocity and temperature distributions are as follows:

$$u = 0 = v, T = T_h \text{ for } 0 \le z \le h \text{ and } t \le 0,$$
$$u = U(t),\ v = 0,$$
$$T = T_h + (T_0 - T_h)\frac{t}{t_0} \text{ at } z = 0 \text{ for } t > 0, \quad (4)$$
$$u = 0 = v, T = T_h \text{ at } z = h \text{ for } t > 0.$$

It has been shown by Cogley et al.[18] that in the optically thin limit for a non-gray gas near

equilibrium, the following relation holds

$$\frac{\partial q_r}{\partial z} = 4(T - T_h)\int_0^\infty K_{\lambda_h}\left(\frac{\partial e_{\lambda p}}{\partial T}\right)_h d\lambda,$$

(5)

where K_λ is the absorption coefficient, λ is the wave length, $e_{\lambda p}$ is the Plank's function and subscript 'h' indicates that all quantities have been evaluated at the temperature T_h which is the temperature of the walls at time $t \le 0$. Thus our study is limited to small difference of wall temperature to the fluid temperature.

On the use of the equation (5), equation (3) becomes

$$\rho c_p \frac{\partial T}{\partial t} = k\frac{\partial^2 T}{\partial z^2} - 4(T - T_h)I,$$

(6)

where

$$I = \int_0^\infty K_{\lambda_h}\left(\frac{\partial e_{\lambda p}}{\partial T}\right)_h d\lambda.$$

(7)

Introducing non-dimensional variables

$$\eta = \frac{z}{h},\ \tau = \frac{\nu t}{h^2},\ (u_1, v_1) = \frac{(u,v)}{u_0},\ \theta = \frac{T - T_h}{T_0 - T_h},$$

$$U(t) = u_0 f(\tau),$$

(8)

equations (1), (2) and (6) become

$$\frac{\partial u_1}{\partial \tau} - 2K^2 v_1 = \frac{\partial^2 u_1}{\partial \eta^2} + Gr\theta - M^2 u_1,$$

(9)

$$\frac{\partial v_1}{\partial \tau} + 2K^2 u_1 = \frac{\partial^2 v_1}{\partial \eta^2} - M^2 v_1,$$

(10)

$$Pr\frac{\partial \theta}{\partial \tau} = \frac{\partial^2 \theta}{\partial \eta^2} - R\theta,$$

(11)

where $M^2 = \dfrac{\sigma B_0^2 h^2}{\rho\nu}$ is the magnetic parameter, $R = \dfrac{4Ih^2}{k}$ the radiation parameter, $Gr = \dfrac{g\beta^*(T_0 - T_h)h^2}{\nu u_0}$ the Grashof number and $Pr = \dfrac{\rho\nu c_p}{k}$ the Prandtl number.

The corresponding initial and boundary conditions for u_1 and θ are

$$u_1 = 0 = v_1, \theta = 0 \text{ for } 0 \le \eta \le 1 \text{ and } \tau \le 0,$$

$$u_1 = f(\tau),\ v_1 = 0,\ \theta = \tau \text{ at } \eta = 0 \text{ for } \tau > 0,$$

(12)

$$u_1 = 0 = v_1,\ \theta = 0 \text{ at } \eta = 1 \text{ for } \tau > 0.$$

Combining equations (9) and (10), we get

$$\frac{\partial F}{\partial \tau} = \frac{\partial^2 F}{\partial \eta^2} + Gr\theta - \lambda^2 F,$$

(13)

where

$$F = u_1 + iv_1,\ \lambda^2 = M^2 + 2iK^2 \text{ and } i = \sqrt{-1}.$$

(14)

The corresponding boundary conditions for F and θ are

$$F = 0, \theta = 0 \text{ for } 0 \le \eta \le 1 \text{ and } \tau \le 0,$$

$$F = f(\tau), \theta = \tau \text{ at } \eta = 0 \text{ for } \tau > 0,$$

(15)

$$F = 0, \theta = 0 \text{ at } \eta = 1 \text{ for } \tau > 0.$$

Taking Laplace transformation, the equations (13) and (11) become

$$s\bar{F} = \frac{d^2\bar{F}}{d\eta^2} + Gr\bar{\theta} - \lambda^2\bar{F},$$

(16)

$$Prs\bar{\theta} = \frac{d^2\bar{\theta}}{d\eta^2} - R\bar{\theta},$$

(17)

where

$$\bar{F}(\eta, s) = \int_0^\infty F(\eta,\tau)e^{-s\tau}\,d\tau$$

and $\bar{\theta}(\eta, s) = \int_0^\infty \theta(\eta,\tau)e^{-s\tau}\,d\tau.$

(18)

The corresponding boundary conditions for $\bar{F}$ and $\bar{\theta}$ are

$$\bar{F}(0,s) = f(s),\ \bar{\theta}(0,s) = \frac{1}{s^2},$$

$$\bar{F}(1,s) = 0,\ \bar{\theta}(1,s) = 0.$$

(19)

where $f(s)$ is the Laplace transform of the function $f(\tau)$.

The solution of the equations (16) and (17) subject to the boundary conditions (19) are given by

$$\bar{\theta}(\eta, s) = \begin{cases} \dfrac{1}{s^2}\dfrac{\sinh\sqrt{sPr + R}(1-\eta)}{\sinh\sqrt{sPr + R}} & \text{for } Pr \ne 1 \\ \dfrac{1}{s^2}\dfrac{\sinh\sqrt{s + R}(1-\eta)}{\sinh\sqrt{s + R}} & \text{for } Pr = 1, \end{cases}$$

(20)

$$\bar{F}(\eta,s)=\begin{cases} f(s)\dfrac{\sinh\sqrt{s+\lambda^2}(1-\eta)}{\sinh\sqrt{s+\lambda^2}} \\ +\dfrac{Gr}{(Pr-1)(s+b)s^2} \\ \times\left[\dfrac{\sinh\sqrt{s+\lambda^2}(1-\eta)}{\sinh\sqrt{s+\lambda^2}}\right. \\ \left.-\dfrac{\sinh\sqrt{sPr+R}(1-\eta)}{\sinh\sqrt{sPr+R}}\right] & \text{for } Pr\neq 1 \\ f(s)\dfrac{\sinh\sqrt{s+\lambda^2}(1-\eta)}{\sinh\sqrt{s+\lambda^2}} \\ +\dfrac{Gr}{(R-\lambda^2)s^2} \\ \times\left[\dfrac{\sinh\sqrt{s+\lambda^2}(1-\eta)}{\sinh\sqrt{s+\lambda^2}}\right. & \text{for } Pr=1, \\ \left.-\dfrac{\sinh\sqrt{s+R}(1-\eta)}{\sinh\sqrt{s+R}}\right] \end{cases}$$

(21)

where $b=\dfrac{R-\lambda^2}{Pr-1}$.

Now, we consider the following cases:

(i) **When one of the wall $(\eta=0)$ started impulsively:**

In this case $f(\tau)=1$, i.e. $f(s)=\dfrac{1}{s}$. The inverse transforms of equations (20) and (21) give the solution for the temperature and the velocity distributions as

$$\theta(\eta,\tau)=\begin{cases} \tau\dfrac{\sinh\sqrt{R}(1-\eta)}{\sinh\sqrt{R}} \\ +\dfrac{Pr}{2\sqrt{R}\sinh^2\sqrt{R}} \\ \times\left[(1-\eta)\cosh\sqrt{R}(1-\eta)\sinh\sqrt{R}\right. \\ \left.-\sinh\sqrt{R}(1-\eta)\cosh\sqrt{R}\right] \\ +2\sum_{n=0}^{\infty}n\pi\dfrac{e^{s_1\tau}}{s_1^2\,Pr}\sin n\pi\eta & \text{for } Pr\neq 1 \\ \tau\dfrac{\sinh\sqrt{R}(1-\eta)}{\sinh\sqrt{R}} \\ +\dfrac{1}{2\sqrt{R}\sinh^2\sqrt{R}} \\ \times\left[(1-\eta)\cosh\sqrt{R}(1-\eta)\sinh\sqrt{R}\right. \\ \left.-\sinh\sqrt{R}(1-\eta)\cosh\sqrt{R}\right] \\ +2\sum_{n=0}^{\infty}n\pi\dfrac{e^{s_1\tau}}{s_1^2}\sin n\pi\eta & \text{for } Pr=1, \end{cases}$$

(22)

$$F(\eta,\tau)=\begin{cases} \dfrac{\sinh\lambda(1-\eta)}{\sinh\lambda} \\ +2\sum_{n=0}^{\infty}n\pi\dfrac{e^{s_2\tau}}{s_2}\sin n\pi\eta & \text{for } Pr\neq 1 \\ +F_1(\eta,\tau,\lambda,Pr,\sqrt{R}) \\ \dfrac{\sinh\lambda(1-\eta)}{\sinh\lambda} \\ +2\sum_{n=0}^{\infty}n\pi\dfrac{e^{s_2\tau}}{s_2}\sin n\pi\eta & \text{for } Pr=1, \\ +F_2(\eta,\tau,\lambda,\sqrt{R}) \end{cases}$$

(23)

where

$$F_1(\eta,\tau,\lambda,Pr,\sqrt{R})$$
$$=\frac{Gr}{Pr-1}\left[\frac{1}{b^2}(\tau b-1)\left\{\frac{\sinh\lambda(1-\eta)}{\sinh\lambda}-\frac{\sinh\sqrt{R}(1-\eta)}{\sinh\sqrt{R}}\right\}\right.$$
$$+\frac{1}{2b\lambda\sinh^2\lambda}\{(1-\eta)\cosh\lambda(1-\eta)\sinh\lambda-\sinh\lambda(1-\eta)\cosh\lambda\}$$
$$-\frac{Pr}{2b\sqrt{R}\sinh^2\sqrt{R}}\{(1-\eta)\cosh\sqrt{R}(1-\eta)\sinh\sqrt{R}-\sinh\sqrt{R}(1-\eta)\cosh\sqrt{R}\}$$
$$\left.+2\sum_{n=0}^{\infty}n\pi\left\{\frac{e^{s_2\tau}}{s_2^2(s_2+b)}-\frac{e^{s_1\tau}}{s_1^2(s_1+b)Pr}\right\}\sin n\pi\eta\right],$$

$$F_2(\eta,\tau,\lambda,\sqrt{R})$$
$$=\frac{Gr}{R-\lambda^2}\left[\tau\left\{\frac{\sinh\lambda(1-\eta)}{\sinh\lambda}-\frac{\sinh\sqrt{R}(1-\eta)}{\sinh\sqrt{R}}\right\}\right.$$
$$+\frac{1}{2\lambda\sinh^2\lambda}\{(1-\eta)\cosh\lambda(1-\eta)\sinh\lambda-\sinh\lambda(1-\eta)\cosh\lambda\}$$

(24)

$$-\frac{1}{2\sqrt{R}\sinh^2\sqrt{R}}\{(1-\eta)\cosh\sqrt{R}(1-\eta)\sinh\sqrt{R}-\sinh\sqrt{R}(1-\eta)\cosh\sqrt{R}\}$$
$$\left.+2\sum_{n=0}^{\infty}n\pi\left\{\frac{e^{s_2\tau}}{s_2^2}-\frac{e^{s_1\tau}}{s_1^2}\right\}\sin n\pi\eta\right],$$

$$s_1=-\frac{(n^2\pi^2+R)}{Pr},\quad s_2=-(n^2\pi^2+\lambda^2),$$

λ is given by (14). On separating into a real and

imaginary parts one can easily obtain the velocity components u_1 and v_1 from equation (23).

For large time τ, equations (22) and (23) become

$$\theta(\eta,\tau)=\begin{cases}\tau\dfrac{\sinh\sqrt{R}(1-\eta)}{\sinh\sqrt{R}}+\dfrac{Pr}{2\sqrt{R}\sinh^2\sqrt{R}}\times\Big[(1-\eta)\cosh\sqrt{R}(1-\eta)\sinh\sqrt{R}-\sinh\sqrt{R}(1-\eta)\cosh\sqrt{R}\Big] & \text{for } Pr\neq 1\\ \tau\dfrac{\sinh\sqrt{R}(1-\eta)}{\sinh\sqrt{R}}+\dfrac{1}{2\sqrt{R}\sinh^2\sqrt{R}}\times\Big[(1-\eta)\cosh\sqrt{R}(1-\eta)\sinh\sqrt{R}-\sinh\sqrt{R}(1-\eta)\cosh\sqrt{R}\Big] & \text{for } Pr=1,\end{cases}$$

(25)

$$F(\eta,\tau)=\begin{cases}\dfrac{\sinh\lambda(1-\eta)}{\sinh\lambda}+F_1(\eta,\tau,\lambda,Pr,\sqrt{R}) & \text{for } Pr\neq 1\\ \dfrac{\sinh\lambda(1-\eta)}{\sinh\lambda}+F_2(\eta,\tau,\lambda,\sqrt{R}) & \text{for } Pr=1,\end{cases}$$

(26)

where

$$F_1(\eta,\tau,\lambda,Pr,\sqrt{R})=\frac{Gr}{Pr-1}\Big[\frac{1}{b^2}(\tau b-1)\Big\{\frac{\sinh\lambda(1-\eta)}{\sinh\lambda}-\frac{\sinh\sqrt{R}(1-\eta)}{\sinh\sqrt{R}}\Big\}+\frac{1}{2b\lambda\sinh^2\lambda}\{(1-\eta)\cosh\lambda(1-\eta)\sinh\lambda-\sinh\lambda(1-\eta)\cosh\lambda\}-\frac{Pr}{2b\sqrt{R}\sinh^2\sqrt{R}}\{(1-\eta)\cosh\sqrt{R}(1-\eta)\sinh\sqrt{R}-\sinh\sqrt{R}(1-\eta)\cosh\sqrt{R}\}\Big],$$

$$F_2(\eta,\tau,\lambda,\sqrt{R})=\frac{Gr}{R-\lambda^2}\Big[\tau\Big\{\frac{\sinh\lambda(1-\eta)}{\sinh\lambda}-\frac{\sinh\sqrt{R}(1-\eta)}{\sinh\sqrt{R}}\Big\}+\frac{1}{2\lambda\sinh^2\lambda}\{(1-\eta)\cosh\lambda(1-\eta)\sinh\lambda-\sinh\lambda(1-\eta)\cosh\lambda\}-\frac{1}{2\sqrt{R}\sinh^2\sqrt{R}}\{(1-\eta)\cosh\sqrt{R}(1-\eta)\sinh\sqrt{R}-\sinh\sqrt{R}(1-\eta)\cosh\sqrt{R}\}\Big],$$

(27)

λ is given by (14).

(ii) When one of the wall $(\eta=0)$ started accelerately:

In this case $f(\tau)=\tau$, i.e. $f(s)=\dfrac{1}{s^2}$. The inverse transforms of equations (20) and (21) yield

$$\theta(\eta,\tau)=\begin{cases}\tau\dfrac{\sinh\sqrt{R}(1-\eta)}{\sinh\sqrt{R}}+\dfrac{Pr}{2\sqrt{R}\sinh^2\sqrt{R}}\times\Big[(1-\eta)\cosh\sqrt{R}(1-\eta)\sinh\sqrt{R}-\sinh\sqrt{R}(1-\eta)\cosh\sqrt{R}\Big]+2\sum_{n=0}^{\infty}n\pi\dfrac{e^{s_1\tau}}{s_1^2Pr}\sin n\pi\eta & \text{for } Pr\neq 1\\ \tau\dfrac{\sinh\sqrt{R}(1-\eta)}{\sinh\sqrt{R}}+\dfrac{1}{2\sqrt{R}\sinh^2\sqrt{R}}\times\Big[(1-\eta)\cosh\sqrt{R}(1-\eta)\sinh\sqrt{R}-\sinh\sqrt{R}(1-\eta)\cosh\sqrt{R}\Big]+2\sum_{n=0}^{\infty}n\pi\dfrac{e^{s_1\tau}}{s_1^2}\sin n\pi\eta & \text{for } Pr=1,\end{cases}$$

(28)

$$F(\eta,\tau)=\begin{cases}\tau\dfrac{\sinh\lambda(1-\eta)}{\sinh\lambda}+\dfrac{1}{2\lambda\sinh^2\lambda}\times\{(1-\eta)\cosh\lambda(1-\eta)\sinh\lambda-\sinh\lambda(1-\eta)\cosh\lambda\}+2\sum_{n=0}^{\infty}n\pi\dfrac{e^{s_2\tau}}{s_2^{\,2}}\sin n\pi\eta+F_1(\eta,\tau,\lambda,Pr,\sqrt{R}) & \text{for } Pr\neq 1\\ \tau\dfrac{\sinh\lambda(1-\eta)}{\sinh\lambda}+\dfrac{1}{2\lambda\sinh^2\lambda}\times\{(1-\eta)\cosh\lambda(1-\eta)\sinh\lambda-\sinh\lambda(1-\eta)\cosh\lambda\}+2\sum_{n=0}^{\infty}n\pi\dfrac{e^{s_2\tau}}{s_2^{\,2}}\sin n\pi\eta+F_2(\eta,\tau,\lambda,\sqrt{R}) & \text{for } Pr=1,\end{cases}$$

(29)

where λ is given by (14), $F_1(\eta,\tau,\lambda,Pr,\sqrt{R})$, $F_2(\eta,\tau,\lambda,\sqrt{R})$, s_1 and s_2 are given by (24). On separating into a real and imaginary parts one can easily obtain the velocity components u_1 and v_1 from equation (29).

For large time τ, equations (28) and (29) become

$$\theta(\eta,\tau)=\begin{cases}\tau\dfrac{\sinh\sqrt{R}(1-\eta)}{\sinh\sqrt{R}}+\dfrac{Pr}{2\sqrt{R}\sinh^2\sqrt{R}}\times\left[(1-\eta)\cosh\sqrt{R}(1-\eta)\sinh\sqrt{R}-\sinh\sqrt{R}(1-\eta)\cosh\sqrt{R}\right] & \text{for } Pr\neq 1\\ \tau\dfrac{\sinh\sqrt{R}(1-\eta)}{\sinh\sqrt{R}}+\dfrac{1}{2\sqrt{R}\sinh^2\sqrt{R}}\times\left[(1-\eta)\cosh\sqrt{R}(1-\eta)\sinh\sqrt{R}-\sinh\sqrt{R}(1-\eta)\cosh\sqrt{R}\right] & \text{for } Pr=1,\end{cases}$$

(30)

$$F(\eta,\tau)=\begin{cases}\tau\dfrac{\sinh\lambda(1-\eta)}{\sinh\lambda}+\dfrac{1}{2\lambda\sinh^2\lambda}\times\{(1-\eta)\cosh\lambda(1-\eta)\sinh\lambda-\sinh\lambda(1-\eta)\cosh\lambda\}+F_1(\eta,\tau,\lambda,Pr,\sqrt{R}) & \text{for } Pr\neq 1\\ \tau\dfrac{\sinh\lambda(1-\eta)}{\sinh\lambda}+\dfrac{1}{2\lambda\sinh^2\lambda}\times\{(1-\eta)\cosh\lambda(1-\eta)\sinh\lambda-\sinh\lambda(1-\eta)\cosh\lambda\}+F_2(\eta,\tau,\lambda,\sqrt{R}) & \text{for } Pr=1,\end{cases}$$

(31)

where λ is given by (14), $F_1(\eta,\tau,\lambda,Pr,\sqrt{R})$ and $F_2(\eta,\tau,\lambda,\sqrt{R})$ are given by (27).

III. RESULTS AND DISCUSSION

We have presented the non-dimensional velocity and temperature distributions for several values of magnetic parameter M^2, rotation parameter K^2, Grashof number Gr, radiation parameter R, Prandtl number Pr and time τ in Figs.2-16 for both the impulsive as well as the accelerated motion of one of the walls. It is seen from Fig.2 that the primary velocity u_1 decreases for both the impulsive and the accelerated motion of one of the walls with an increase in magnetic parameter M^2. The presence of a magnetic field normal to the flow in an electrically conducting fluid introduces a Lorentz force which acts against the flow. This resistive force tends to slow down the flow and hence the fluid velocities decrease with an increase in magnetic parameter. This trend is consistent with many classical studies on magneto-convection flow. Fig.3 reveals that the primary velocity u_1 decreases near the wall $(\eta=0)$ while it increases in the vicinity of the wall $(\eta=1)$ for both the impulsive and the accelerated motion of one of the walls with an increase in rotation parameter K^2. The rotation parameter K^2 defines the relative magnitude of the Coriolis force and the viscous force in the regime, therefore it is clear that the high magnitude Coriolis forces are counter-productive for the primary velocity. It is observed from Fig.4 that the primary velocity u_1 decreases near the wall $(\eta=0)$ while it

increases away from that wall for both the impulsive and the accelerated motion of one of the walls with an increase in Grashof number Gr. For $R<1$, thermal conduction exceeds thermal radiation and for $R>1$, this situation is reversed. For $R=1$, the contribution from both modes is equal. It is seen from Fig.5 that an increase in radiation parameter R leads to a decrease in primary velocity for both impulsive and accelerated motion of one of the walls. Fig.6 shows that the primary velocity decreases for both impulsive as well as accelerated motion of one of the walls with an increase in Prandtl number Pr. Physically, this is true because the increase in the Prandtl number is due to increase in the viscosity of the fluid which makes the fluid thick and hence causes a decrease in the velocity of the fluid. It is revealed from Fig.7 that the primary velocity u_1 increases near the wall $(\eta=0)$ and decreases away from the wall for the impulsive motion whereas it increases for the accelerated motion with an increase in time τ. It is noted from Figs. 2-7 that the primary velocity for the impulsive motion is greater than that of the accelerated motion near the wall $(\eta=0)$. It is observed from Fig.8, Fig.10 and Fig.11 that the secondary velocity v_1 increases for both impulsive and accelerated motion of one of the walls with an increase in either magnetic parameter M^2 or Grashof number Gr or radiation parameter R. It means that magnetic field, buoyancy force and radiation tend to enhance the secondary velocity. It is illustrated from Fig.9 and Fig.12 that the secondary velocity v_1 increases near the wall $(\eta=0)$ while it decreases near the wall $(\eta=1)$ for both impulsive and accelerated motion of one of the walls with an increase in either rotation parameter K^2 or Prandtl number Pr. Fig.13 reveals that the secondary velocity v_1 decreases for the impulsive motion whereas it increases for the accelerated motion of one of the walls with an increase in time τ. From Figs.8-13, it is interesting to note that the secondary velocity for the impulsive motion is greater than that of the accelerated motion of one of the walls. Further, from Figs.2-13 it is seen that the value of the fluid velocity components become negative at the middle region between two walls which indicates that there occurs a reverse flow at that region. Physically this is possible as the motion of the fluid is due to the wall motion in the upward direction against the gravitational field.

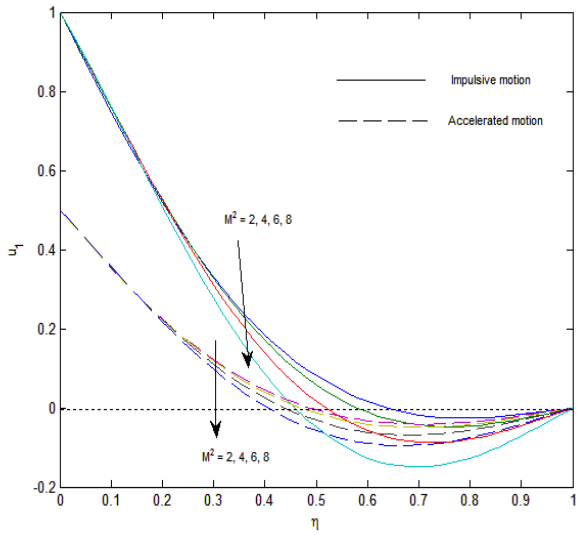

Fig.2: Primary velocity for M^2 with $R=1$, $K^2=5$, $Pr=0.03$, $Gr=5$ and $\tau=0.5$

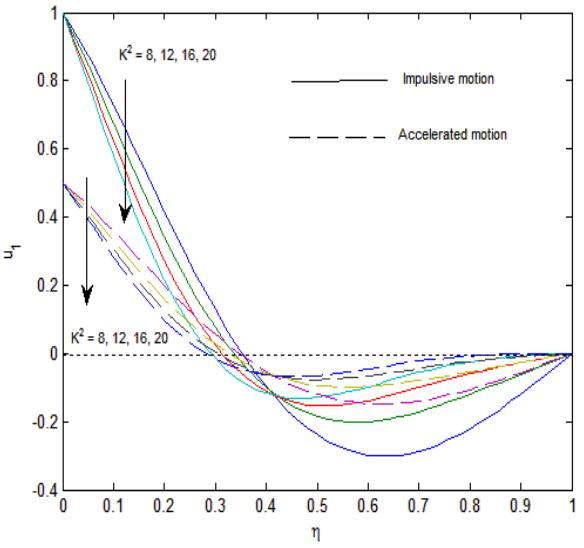

Fig.3: Primary velocity for K^2 with $R=1$, $M^2=15$, $Pr=0.03$, $Gr=5$ and $\tau=0.5$

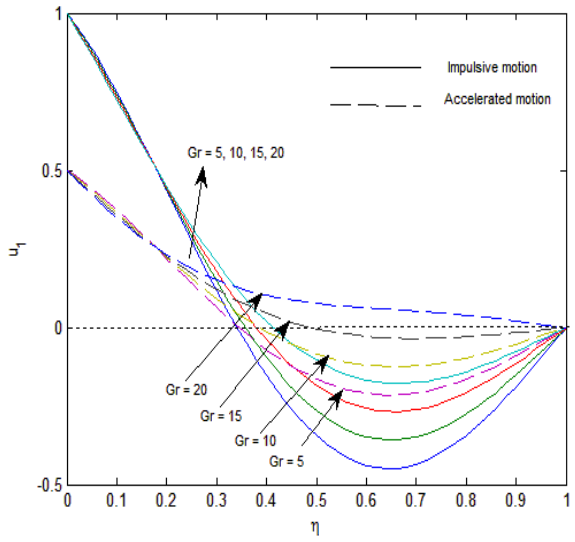

Fig.4: Primary velocity for Gr with $R=1$, $M^2=15$, $Pr=0.03$, $K^2=5$ and $\tau=0.5$

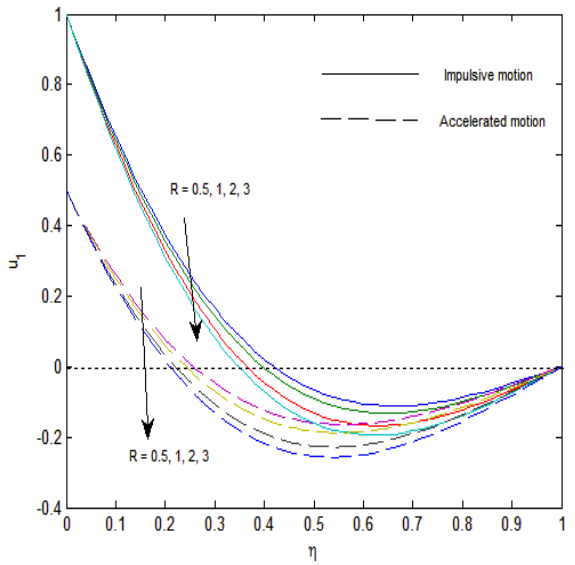

Fig.5: Primary velocity for R with $Gr=15$, $M^2=2$, $Pr=0.03$, $K^2=5$ and $\tau=0.5$

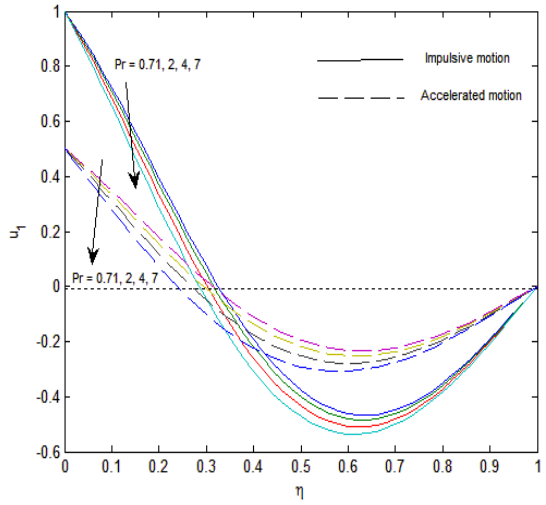

Fig.6: Primary velocity for Pr with $R=1$, $M^2=15$, $Gr=5$, $K^2=5$ and $\tau=0.5$

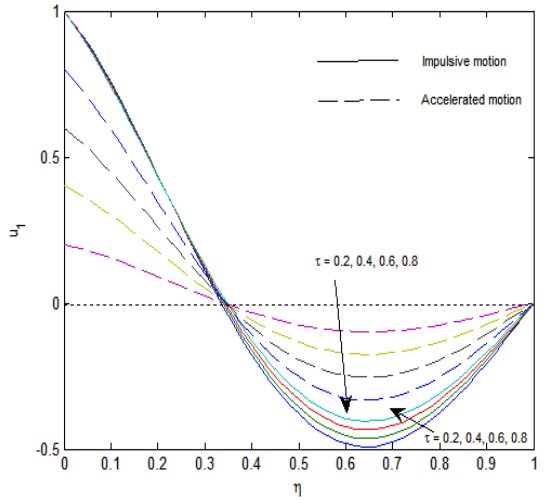

Fig.7: Primary velocity for τ with $R=1$, $M^2=15$, $Gr=5$, $K^2=5$ and $Pr=0.03$

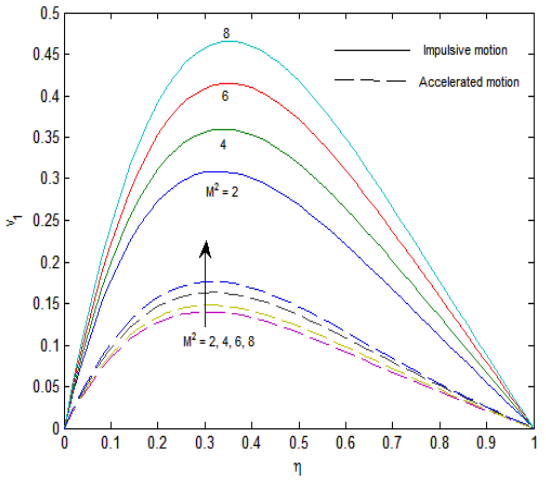

Fig.8: Secondary velocity for M^2 with $R=1$, $K^2=5$, $Pr=0.03$, $Gr=5$ and $\tau=0.5$

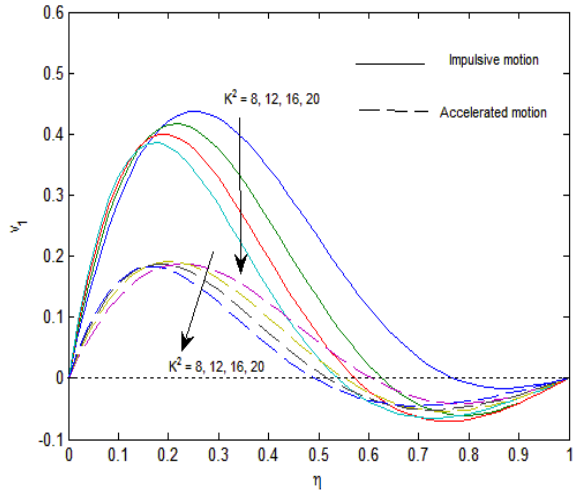

Fig.9: Secondary velocity for K^2 with $R=1$, $M^2=15$, $Pr=0.03$, $Gr=5$ and $\tau=0.5$

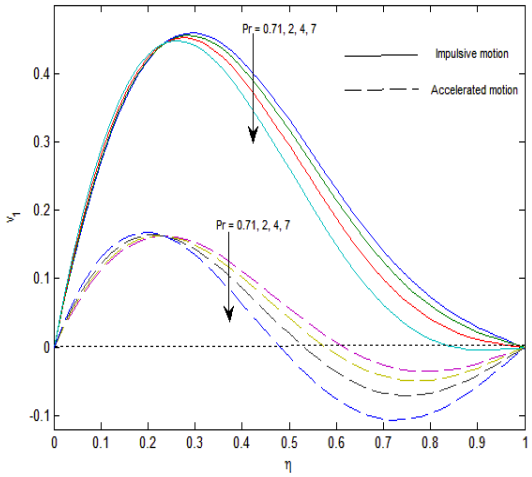

Fig.12: Secondary velocity for Pr with $R=1$, $M^2=15$, $Gr=5$, $K^2=5$ and $\tau=0.5$

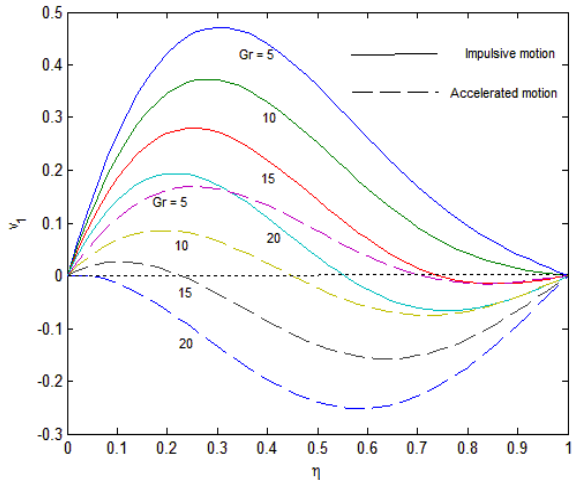

Fig.10: Secondary velocity for Gr with $R=1$, $M^2=15$, $Pr=0.03$, $K^2=5$ and $\tau=0.5$

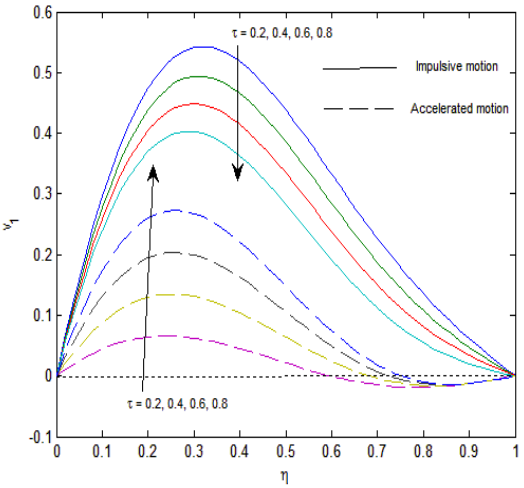

Fig.13: Secondary velocity for τ with $R=1$, $M^2=15$, $Gr=5$, $K^2=5$ and $Pr=0.03$

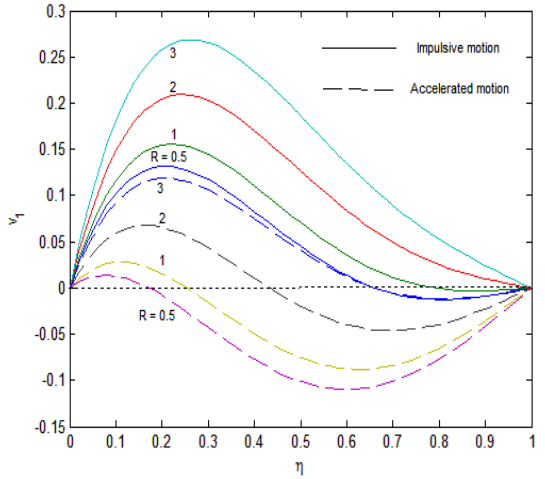

Fig.11: Secondary velocity for R with $Gr=15$, $M^2=2$, $Pr=0.03$, $K^2=5$ and $\tau=0.5$

The effects of radiation parameter R, Prandtl number Pr and time τ on the temperature distribution have been shown in Figs.14-16. It is observed from Fig.14 that the fluid temperature $\theta(\eta,\tau)$ decreases with an increase in radiation parameter R. This result qualitatively agrees with expectations, since the effect of radiation decrease the rate of energy transport to the fluid, thereby decreasing the temperature of the fluid. Fig.15 shows that the fluid temperature $\theta(\eta,\tau)$ decreases with an increase in Prandtl number Pr. Prandtl number Pr is the ratio of viscosity to thermal diffusivity. An increase in thermal diffusivity leads to a decrease in Prandtl number. Therefore, thermal diffusion has a tendency to reduce the fluid temperature. It is revealed from Fig.16 that an increase in time τ leads to rise in the fluid

temperature distribution $\theta(\eta,\tau)$. It indicates that there is an enhancement in fluid temperature as time progresses.

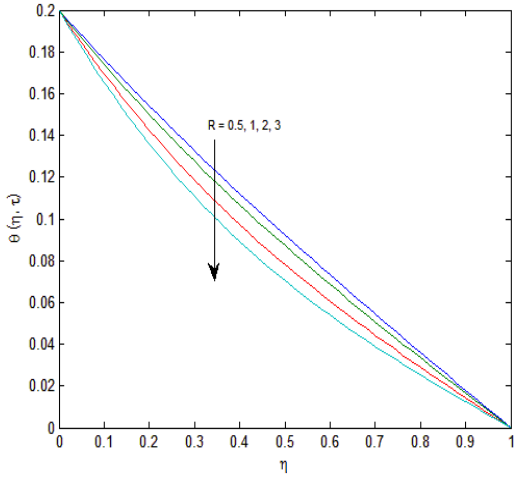

Fig.14: Temperature profiles for different R with $\tau = 0.2$ and $Pr = 0.03$

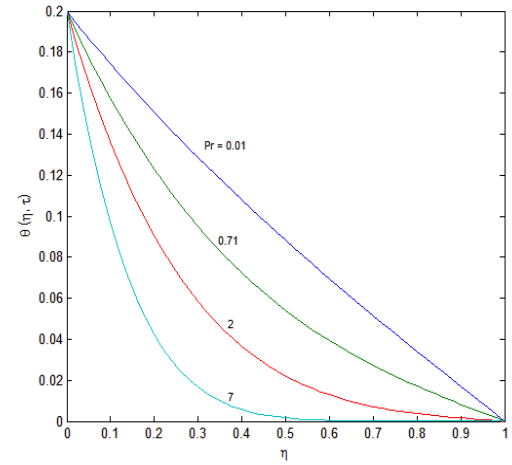

Fig.15: Temperature profiles for different Pr with $\tau = 0.2$ and $R = 1$

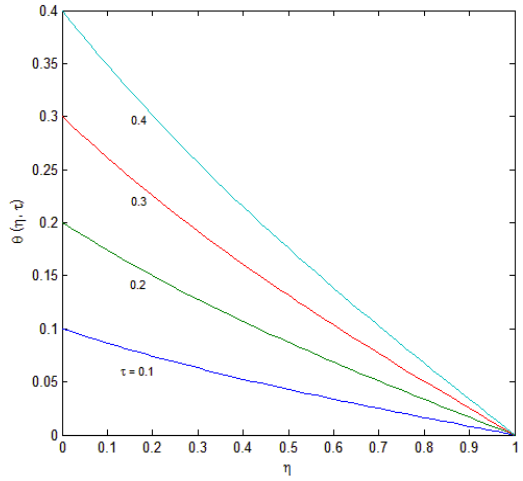

Fig.16: Temperature profiles for different τ with $R = 1$ and $Pr = 0.03$

For the impulsive motion, the non-dimensional shear stresses at the walls $(\eta = 0)$ and $(\eta = 1)$ are respectively obtained as follows:

$$\tau_{x_0} + i\tau_{y_0} = \left(\frac{\partial F}{\partial \eta}\right)_{\eta=0}$$

$$= \begin{cases} -\lambda \coth \lambda \\ +2\sum_{n=0}^{\infty} n^2 \pi^2 \frac{e^{s_2 \tau}}{s_2} & \text{for } Pr \neq 1 \\ +G_1(0,\tau,\lambda,Pr,\sqrt{R}) \\ \\ -\lambda \coth \lambda \\ +2\sum_{n=0}^{\infty} n^2 \pi^2 \frac{e^{s_2 \tau}}{s_2} & \text{for } Pr = 1, \\ +G_2(0,\tau,\lambda,\sqrt{R}) \end{cases}$$

(32)

$$\tau_{x_1} + i\tau_{y_1} = \left(\frac{\partial F}{\partial \eta}\right)_{\eta=1}$$

$$= \begin{cases} -\lambda\, cosech\lambda \\ +2\sum_{n=0}^{\infty} n^2 \pi^2 (-1)^n \frac{e^{s_2 \tau}}{s_2} & \text{for } Pr \neq 1 \\ +G_1(1,\tau,\lambda,Pr,\sqrt{R}) \\ \\ -\lambda\, cosech\lambda \\ +2\sum_{n=0}^{\infty} n^2 \pi^2 (-1)^n \frac{e^{s_2 \tau}}{s_2} & \text{for } Pr = 1, \\ +G_2(1,\tau,\lambda,\sqrt{R}) \end{cases}$$

(33)

where

$$G_1(0,\tau,\lambda,Pr,\sqrt{R}) = \frac{Gr}{Pr-1}\left[\frac{1}{b^2}(\tau b-1)\right.$$
$$\times\left(\sqrt{R}\coth\sqrt{R}-\lambda\coth\lambda\right)$$
$$+\frac{1}{2b\lambda\sinh^2\lambda}\left(\lambda-\cosh\lambda\sinh\lambda\right)$$
$$-\frac{Pr}{2b\sqrt{R}\sinh^2\sqrt{R}}\left(\sqrt{R}-\cosh\sqrt{R}\sinh\sqrt{R}\right)$$
$$\left.+2\sum_{n=0}^{\infty}n^2\pi^2\left\{\frac{e^{s_2\tau}}{s_2^{\,2}(s_2+b)}-\frac{e^{s_1\tau}}{s_1^{\,2}(s_1+b)Pr}\right\}\right],$$

$$G_1(1,\tau,\lambda,Pr,\sqrt{R}) = \frac{Gr}{Pr-1}\left[\frac{1}{b^2}(\tau b-1)\right.$$
$$\times\left(\sqrt{R}\,cosech\sqrt{R}-\lambda\,cosech\lambda\right)$$
$$+\frac{1}{2b\lambda\sinh^2\lambda}\left(\lambda\cosh\lambda-\sinh\lambda\right)$$
$$-\frac{Pr}{2b\sqrt{R}\sinh^2\sqrt{R}}\left(\sqrt{R}\cosh\sqrt{R}-\sinh\sqrt{R}\right)$$
$$\left.+2\sum_{n=0}^{\infty}n^2\pi^2(-1)^n\left\{\frac{e^{s_2\tau}}{s_2^{\,2}(s_2+b)}-\frac{e^{s_1\tau}}{s_1^{\,2}(s_1+b)Pr}\right\}\right],$$

(34)

$$G_2(0,\tau,\lambda,\sqrt{R}) = \frac{Gr}{R-\lambda^2}\left[\tau\right.$$
$$\times\left(\sqrt{R}\coth\sqrt{R}-\lambda\coth\lambda\right)$$
$$+\frac{1}{2\lambda\sinh^2\lambda}\left(\lambda-\cosh\lambda\sinh\lambda\right)$$
$$-\frac{1}{2\sqrt{R}\sinh^2\sqrt{R}}\left(\sqrt{R}-\cosh\sqrt{R}\sinh\sqrt{R}\right)$$
$$\left.+2\sum_{n=0}^{\infty}n^2\pi^2\left\{\frac{e^{s_2\tau}}{s_2^{\,2}}-\frac{e^{s_1\tau}}{s_1^{\,2}}\right\}\right],$$

$$G_2(1,\tau,\lambda,\sqrt{R}) = \frac{Gr}{R-\lambda^2}\left[\tau\right.$$
$$\times\left(\sqrt{R}\,cosech\sqrt{R}-\lambda\,cosech\lambda\right)$$
$$+\frac{1}{2\lambda\sinh^2\lambda}\left(\lambda\cosh\lambda-\sinh\lambda\right)$$
$$-\frac{1}{2\sqrt{R}\sinh^2\sqrt{R}}\left(\sqrt{R}\cosh\sqrt{R}-\sinh\sqrt{R}\right)$$
$$\left.+2\sum_{n=0}^{\infty}n^2\pi^2(-1)^n\left\{\frac{e^{s_2\tau}}{s_2^{\,2}}-\frac{e^{s_1\tau}}{s_1^{\,2}}\right\}\right],$$

λ is given by (14), s_1 and s_2 are given by (24).

For the accelerated motion, the non-dimensional shear stresses at the walls $(\eta=0)$ and $(\eta=1)$ are respectively obtained as follows:

$$\tau_{x_0}+i\tau_{y_0} = \left(\frac{\partial F}{\partial\eta}\right)_{\eta=0}$$
$$= \begin{cases} -\tau\lambda\coth\lambda \\ +\frac{1}{2\lambda\sinh^2\lambda}\left(\lambda-\cosh\lambda\sinh\lambda\right) \\ 2\sum_{n=0}^{\infty}n^2\pi^2\frac{e^{s_2\tau}}{s_2^{\,2}} & \text{for } Pr\neq 1 \\ +G_1(0,\tau,\lambda,Pr,\sqrt{R}) \\ \\ -\tau\lambda\coth\lambda \\ +\frac{1}{2\lambda\sinh^2\lambda}\left(\lambda-\cosh\lambda\sinh\lambda\right) \\ 2\sum_{n=0}^{\infty}n^2\pi^2\frac{e^{s_2\tau}}{s_2^{\,2}} & \text{for } Pr=1, \\ +G_2(0,\tau,\lambda,\sqrt{R}) \end{cases}$$

(35)

$$\tau_{x_1}+i\tau_{y_1} = \left(\frac{\partial F}{\partial\eta}\right)_{\eta=1}$$
$$= \begin{cases} -\tau\lambda\,cosech\lambda \\ +\frac{1}{2\lambda\sinh^2\lambda}\left(\lambda\cosh\lambda-\sinh\lambda\right) \\ +2\sum_{n=0}^{\infty}n^2\pi^2(-1)^n\frac{e^{s_2\tau}}{s_2^{\,2}} & \text{for } Pr\neq 1 \\ +G_1(1,\tau,\lambda,Pr,\sqrt{R}) \\ \\ -\tau\lambda\,cosech\lambda \\ +\frac{1}{2\lambda\sinh^2\lambda}\left(\lambda\cosh\lambda-\sinh\lambda\right) \\ +2\sum_{n=0}^{\infty}n^2\pi^2(-1)^n\frac{e^{s_2\tau}}{s_2^{\,2}} & \text{for } Pr=1, \\ +G_2(1,\tau,\lambda,\sqrt{R}) \end{cases}$$

(36)

where λ is given by (14), $G_1(0,\tau,\lambda,Pr,\sqrt{R})$, $G_1(1,\tau,\lambda,Pr,\sqrt{R})$, $G_2(0,\tau,\lambda,\sqrt{R})$ and $G_2(1,\tau,\lambda,\sqrt{R})$ are given by (34).

Numerical results of the non-dimensional shear stresses at the wall $(\eta=0)$ are presented in Figs.17-20 against magnetic parameter M^2 for several values of rotation parameter K^2 and radiation parameter R when $\tau=0.2$, $Gr=5$ and $Pr=0.03$. Figs.17 and 18 show that the absolute value of the shear stress τ_{x_0} at the wall $(\eta=0)$ due to the primary flow increases with an increase in either

rotation parameter K^2 or radiation parameter R whereas it decreases with an increase in magnetic parameter M^2 for both the impulsive and the accelerated motion of one of the walls. It is observed from Figs.19 and 20 that the shear stress τ_{y_0} at the wall $(\eta = 0)$ due to the secondary flow increases with an increase in either rotation parameter K^2 or radiation parameter R or magnetic parameter M^2 for both the impulsive and the accelerated motion of one of the walls. Further, it is observed from Figs.19 and 20 that the shear stress τ_{y_0} at the plate $(\eta = 0)$ due to the secondary flow for the impulsive start of one of the walls is greater than that of the accelerated start.

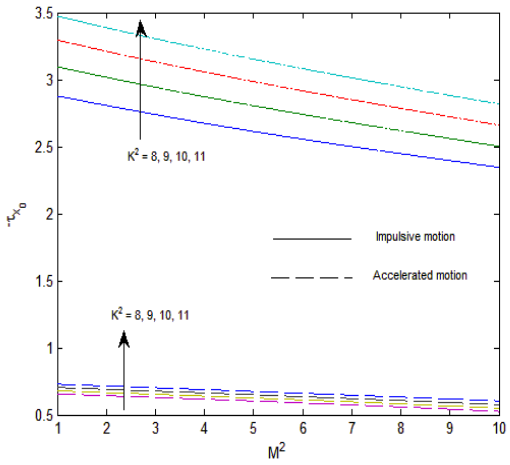

Fig.17: Shear stress τ_{x_0} due to primary flow for different K^2 when $R = 1$

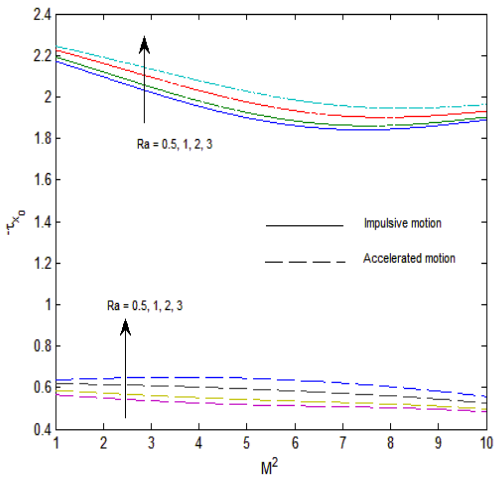

Fig.18: Shear stress τ_{x_0} due to primary flow for different R when $K^2 = 5$

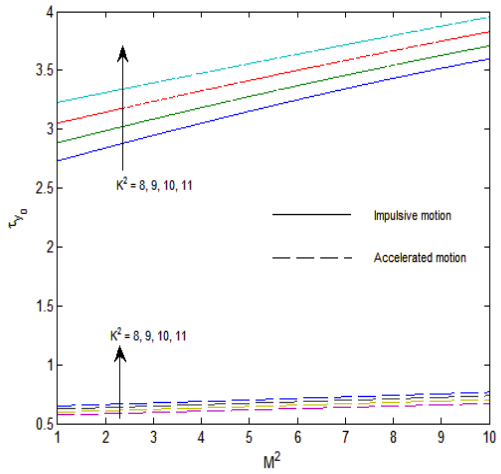

Fig.19: Shear stress τ_{y_0} due to secondary flow for different K^2 when $R = 1$

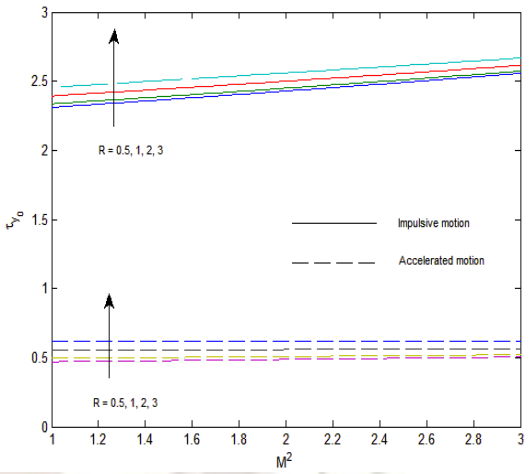

Fig.20: Shear stress τ_{y_0} due to secondary flow for different R when $K^2 = 5$

The rate of heat transfer at the walls $(\eta = 0)$ and $(\eta = 1)$ are respectively given by

$$\theta'(0) = \left.\frac{\partial \theta}{\partial \eta}\right|_{\eta=0}$$

$$= \begin{cases} -\tau\sqrt{R}\coth\sqrt{R} \\ +\dfrac{Pr}{2\sqrt{R}\sinh^2\sqrt{R}} \\ \times\left[\sqrt{R}-\cosh\sqrt{R}\sinh\sqrt{R}\right] \\ +2\sum_{n=0}^{\infty} n^2\pi^2\dfrac{e^{s_1\tau}}{s_1^2 Pr} & \text{for } Pr\neq 1 \\ \\ -\tau\sqrt{R}\coth\sqrt{R} \\ +\dfrac{1}{2\sqrt{R}\sinh^2\sqrt{R}} \\ \times\left[\sqrt{R}-\cosh\sqrt{R}\sinh\sqrt{R}\right] \\ +2\sum_{n=0}^{\infty} n^2\pi^2\dfrac{e^{s_1\tau}}{s_1^2} & \text{for } Pr=1, \end{cases}$$

(37)

$$= \begin{cases} -\tau\sqrt{R}\,\mathrm{cosech}\sqrt{R} \\ +\dfrac{Pr}{2\sqrt{R}\sinh^2\sqrt{R}} \\ \times\left[\sqrt{R}\cosh\sqrt{R}-\sinh\sqrt{R}\right] \\ +2\sum_{n=0}^{\infty} n^2\pi^2(-1)^n\dfrac{e^{s_1\tau}}{s_1^2 Pr} & \text{for } Pr\neq 1 \\ \\ -\tau\sqrt{R}\,\mathrm{cosech}\sqrt{R} \\ +\dfrac{1}{2\sqrt{R}\sinh^2\sqrt{R}} \\ \times\left[\sqrt{R}\cosh\sqrt{R}-\sinh\sqrt{R}\right] \\ +2\sum_{n=0}^{\infty} n^2\pi^2(-1)^n\dfrac{e^{s_1\tau}}{s_1^2} & \text{for } Pr=1, \end{cases}$$

(38)

$$\theta'(1)=\left.\frac{\partial\theta}{\partial\eta}\right|_{\eta=1}$$

where s_1 is given by (24).

Numerical results of the rate of heat transfer $-\theta'(0)$ at the wall $(\eta=0)$ and $-\theta'(1)$ at the wall $(\eta=1)$ against the radiation parameter R are presented in the Table 1 and 2 for several values of Prandtl number Pr and time τ. Table 1 shows that the rate of heat transfer $-\theta'(0)$ increases whereas $-\theta'(1)$ decreases with an increase in Prandtl number Pr. It is observed from Table 2 that the rates of heat transfer $-\theta'(0)$ and $-\theta'(1)$ increase with an increase in time τ. Further, it is seen from Table 1 and 2 that the rate of heat transfer $-\theta'(0)$ increases whereas the rate of heat transfer $-\theta'(1)$ decreases with an increase in radiation parameter R.

Table 1. Rate of heat transfer at the plate $(\eta=0)$ and at the plate $(\eta=1)$

	$-\theta'(0)$				$-\theta'(1)$			
$R \setminus Pr$	0.01	0.71	1	2	0.01	0.71	1	2
0.5	0.23540	0.44719	0.52178	0.72549	0.18277	0.08573	0.05865	0.01529
1.0	0.26555	0.46614	0.53808	0.73721	0.16885	0.08117	0.05599	0.01483
1.5	0.29403	0.48461	0.55407	0.74881	0.15635	0.07690	0.05346	0.01438
2.0	0.32102	0.50262	0.56976	0.76030	0.14509	0.07290	0.05106	0.01394

Table 2. Rate of heat transfer at the plate $(\eta=0)$ and at the plate $(\eta=1)$

	$-\theta'(0)$				$-\theta'(1)$			
$R \setminus \tau$	0.1	0.2	0.3	0.4	0.1	0.2	0.3	0.4
0.5	0.12551	0.24165	0.35779	0.47392	0.08767	0.17980	0.27193	0.36405
1.0	0.14014	0.27144	0.40275	0.53405	0.08110	0.16619	0.25128	0.33637
1.5	0.15398	0.29960	0.44522	0.59084	0.07518	0.15396	0.23273	0.31151
2.0	0.16712	0.32631	0.48550	0.64469	0.06984	0.14292	0.21601	0.28909

IV. CONCLUSION

The radiation effects on MHD free convective Couette flow in a rotating system confined between two infinitely long vertical walls with variable temperature have been studied. Magnetic field and radiation have a retarding influence on the primary velocity whereas they have an accelerating influence on the secondary velocity for both the impulsive as well as the accelerated motion of one of the walls. The effect of the rotation is very important in the velocity field. It is noted that the velocity for the impulsive motion is greater than that of the accelerated motion near the wall $(\eta = 0)$. An increase in either radiation parameter R or Prandtl number Pr leads to fall in the fluid temperature θ. There is an enhancement in fluid temperature as time progresses. Both the rotation and radiation enhance the absolute value of the shear stress τ_{x_0} and the shear stress τ_{y_0} at the wall $(\eta = 0)$ for both the impulsive as well as the accelerated motion of one of the walls. Further, the rate of heat transfer $-\theta'(0)$ at the wall $(\eta = 0)$ increases whereas the rate of heat transfer $-\theta'(1)$ at the wall $(\eta = 1)$ decreases with an increase in radiation parameter R.

REFERENCES

[1] A. K. Singh, Natural Convection in Unsteady Couette Motion, *Defense Science Journal, 38(1)*, 1988, 35-41.

[2] A. K. Singh, and T. Paul, Transient natural convection between two vertical walls heated/cooled asymetrically, *International Journal of Applied Mechanics and Engineering, 11(1)*, 2006, 143-154.

[3] B. K. Jha, A. K. Singh, and H. S. Takhar, Transient free convection flow in a vertical channel due to symmetric heating, *International Journal of Applied Mechanics and Engineering, 8(3)*, 2003, 497-502.

[4] H. M. Joshi, Transient effects in natural convection cooling of vertical parallel plates, *International Communications in Heat and Mass Transfer, 15(2)*, 1988, 227-238.

[5] O. Miyatake, and T. Fujii, Free convection heat transfer between vertical plates - one plate isothermally heated and other thermally insulated, *Heat Transfer – Japanese Research, 1*, 1972, 30-38.

[6] O. Miyatake, H. Tanaka, T. Fujii, and M. Fujii, Natural convection heat transfer between vertical parallel plates- one plate with a uniform heat flux and the other thermally insulated, *Heat Transfer – Japanese Research, 2*, 1973, 25-33.

[7] A. K. Singh, H. R. Gholami, and V. M. Soundalgekar, Transient free convection flow between two vertical parallel plates. *Heat and Mass Transfer, 31(5)*, 1996, 329-331.

[8] B. K. Jha, Natural convection in unsteady MHD Couette flow, Heat and Mass Transfer, *37(4-5)*, 2001, 329-331.

[9] A. Ogulu, and S. Motsa, Radiative heat transfer to magnetohydrodynamic Couette flow with variable wall temperature, *Physica Scripta, 71(4)*, 2005, 336-339.

[10] P. Mebine, Radiation effects on MHD Couette flow with heat transfer between two parallel plates, *Global Journal of Pure and Applied Mathematics, 3(2)*, 2007, 1-12.

[11] B. K. Jha, and A. O. Ajibade, Unsteady free convective Couette flow of heat generating/absorbing fluid, *International Journal of Energy and Technology, 2(12)*, 2010, 1–9.

[12] M. Narahari, Effects of thermal radiation and free convection currents on the unsteady Couette flow between two vertical parallel plates with constant heat flux at one boundary, *WSEAS Transactions on Heat and Mass Transfer, 5(1)*, 2010, 21-30.

[13] A.G. V. Kumar, and S.V.K. Varma, Radiation effects on MHD flow past an impulsively started exponentially accelerated vertical plate with variable temperature in the presence of heat generation, *International Journal of Engineering Science and Technology, 3(4)*, 2011, 2897-2909.

[14] U.S. Rajput, and P.K. Sahu, Transient free convection MHD flow between two long vertical parallel plates with constant temperature and variable mass diffusion, *International Journal of Mathematical Analysis, 5(34)*, 2011, 1665-6671.

[15] U.S. Rajput, and S. Kumar, Rotation and radiation effects on MHD flow past an impulsively started vertical plate with variable temperature, *International Journal of Mathematical Analysis, 5(24)*, 2011, 1155 - 1163.

[16] S. Das, B. C. Sarkar, and R. N. Jana, Radiation effects on free convection MHD Couette flow started exponentially with variable wall temperature in presence of heat generation, *Open Journal of Fluid Dynamics, 2(1)*, 2012, 14-27.

[17] C. Mandal, S. Das, and R. N. Jana, Effect of radiation on transient natural convection flow between two vertical walls, *International Journal of Applied Information Systems, 2(2)*, 2012, 49-56.

[18] A.C. Cogley, W.C. Vincentine, and S.E. Gilles, A differential approximation for radiative transfer in a non-gray gas near equilibrium. *The American Institute of Aeronautics and Astronautics Journal, 6*, 1968, 551-555.